High-pressure structural and elastic properties of Tl2O3

O. Gomis, D. Santamaría-Pérez, J. Ruiz-Fuertes, J. A. Sans, R. Vilaplana, H. M. Ortiz, B. García-Domene, F. J. Manjón, D. Errandonea, P. Rodríguez-Hernández, A. Muñoz, and M. Mollar

Citation: Journal of Applied Physics **116**, 133521 (2014); doi: 10.1063/1.4897241
View online: http://dx.doi.org/10.1063/1.4897241
View Table of Contents: http://scitation.aip.org/content/aip/journal/jap/116/13?ver=pdfcov
Published by the AIP Publishing

High-pressure structural and elastic properties of Tl_2O_3

O. Gomis,[1,a)] D. Santamaría-Pérez,[2,3] J. Ruiz-Fuertes,[2,4] J. A. Sans,[5] R. Vilaplana,[1] H. M. Ortiz,[5,6,b)] B. García-Domene,[2] F. J. Manjón,[5] D. Errandonea,[2] P. Rodríguez-Hernández,[7] A. Muñoz,[7] and M. Mollar[5]

[1]*Centro de Tecnologías Físicas, MALTA Consolider Team, Universitat Politècnica de València, 46022 València, Spain*
[2]*Departamento de Física Aplicada-ICMUV, MALTA Consolider Team, Universidad de Valencia, Edificio de Investigación, C/Dr. Moliner 50, 46100 Burjassot, Spain*
[3]*Earth Sciences Department, University College London, Gower Street, WC1E 6BT London, United kingdom*
[4]*Geowissenschaften, Goethe-Universität, Altenhöferallee 1, 60438 Frankfurt am Main, Germany*
[5]*Instituto de Diseño para la Fabricación y Producción Automatizada, MALTA Consolider Team, Universitat Politècnica de València, 46022 València, Spain*
[6]*CINVESTAV-Departamento de Nanociencia y Nanotecnología, Unidad Querétaro, 76230 Querétaro, Mexico*
[7]*Departamento de Física, Instituto de Materiales y Nanotecnología, MALTA Consolider Team, Universidad de La Laguna, 38205 La Laguna, Tenerife, Spain*

(Received 23 July 2014; accepted 24 September 2014; published online 7 October 2014)

The structural properties of Thallium (III) oxide (Tl_2O_3) have been studied both experimentally and theoretically under compression at room temperature. X-ray powder diffraction measurements up to 37.7 GPa have been complemented with *ab initio* total-energy calculations. The equation of state of Tl_2O_3 has been determined and compared to related compounds. It has been found experimentally that Tl_2O_3 remains in its initial cubic bixbyite-type structure up to 22.0 GPa. At this pressure, the onset of amorphization is observed, being the sample fully amorphous at 25.2 GPa. The sample retains the amorphous state after pressure release. To understand the pressure-induced amorphization process, we have studied theoretically the possible high-pressure phases of Tl_2O_3. Although a phase transition is theoretically predicted at 5.8 GPa to the orthorhombic Rh_2O_3-II-type structure and at 24.2 GPa to the orthorhombic α-Gd_2S_3-type structure, neither of these phases were observed experimentally, probably due to the hindrance of the pressure-driven phase transitions at room temperature. The theoretical study of the elastic behavior of the cubic bixbyite-type structure at high-pressure shows that amorphization above 22 GPa at room temperature might be caused by the mechanical instability of the cubic bixbyite-type structure which is theoretically predicted above 23.5 GPa. © *2014 AIP Publishing LLC*. [http://dx.doi.org/10.1063/1.4897241]

I. INTRODUCTION

Thallium (III) oxide (Tl_2O_3) is a sesquioxide which occurs naturally as a rare mineral named avicennite.[1] Tl_2O_3 crystallizes at ambient conditions in the body-centered cubic bixbyite-type structure with space group (S.G.) Ia-3, No. 206, $Z = 16$.[2–4] Bixbyite-type Tl_2O_3 is isomorphic to the cubic structure of In_2O_3 and several rare-earth sesquioxides. Apart from the bixbyite structure, the corundum-type structure has been reported to be synthesized at high pressures and high temperatures.[5]

Tl_2O_3 can be applied in many technological areas.[6] In particular, it has been used as an electrode in high-efficiency solar cells due to its very low resistivity.[7,8] It has also been studied for optical communication applications because of its strong reflectance in the near infrared region (1300–1500 nm);[9] however, its most promising application is in thallium oxide-based high-temperature superconductors.[10]

Despite its interesting technological applications, Tl_2O_3 is one of the less studied sesquioxides probably because of the poisonous nature of thallium. In particular, contact with moisture and acids may form poisonous soluble thallium compounds, like thallium acetate, whose contact with skin should be avoided.[11] Consequently, many properties of Tl_2O_3 are unknown. In particular, it was long thought that this compound behaves as a metallic conductor;[12–14] however, it has been recently shown that it is a degenerate n-type semiconductor.[15] This result is in good agreement with transport measurements which suggest that n-type conductivity comes from oxygen deficiency in the crystalline lattice.[13,16–18] It is also in good agreement with optical measurements providing a band gap between 1.40 and 2.75 eV.[9,12,16]

Very little is known about the structural and mechanical properties of Tl_2O_3. The bulk moduli of both bixbyite-type and corundum-type structures are unknown. In this context, studies of Tl_2O_3 under compression could help in understanding its physical properties. In this work, we report an experimental and theoretical study of bixbyite-type Tl_2O_3 at room temperature and high-pressure (HP) by means of angle dispersive X-ray diffraction (ADXRD) measurements and *ab initio* calculations. Technical aspects of the experiments and calculations are described in Secs. II and III, respectively. Results are presented and discussed in Sec. IV and conclusions summarized in Sec. V.

[a)]Author to whom correspondence should be addressed. Electronic mail: osgohi@fis.upv.es
[b)]On leave from Departamento de Física, Universidad Distrital "Francisco José de Caldas," 110311 Bogotá, Colombia.

II. EXPERIMENTAL DETAILS

Commercial Tl_2O_3 powder with 99.99% purity (Sigma-Aldrich) was crushed in a mortar with a pestle to obtain a micron-sized powder. XRD measurements performed at 1 atm and room temperature with a Rigaku Ultima IV diffractometer (Cu K_α radiation) confirmed the bixbyite-type structure of Tl_2O_3.

HP-ADXRD experiments at room temperature up to 37.7 GPa were carried out at beamline I15 of the Diamond Light Source using a monochromatic X-ray beam ($\lambda = 0.4246$ Å) and a membrane-type diamond-anvil cell (DAC). Tl_2O_3 powder was loaded in a 150–μm diameter hole of an inconel gasket in a DAC with diamond-culet sizes of 350 μm. A 16:3:1 methanol-ethanol-water mixture was used as pressure-transmitting medium. A strip of gold was placed inside the gasket and used as the pressure sensor. Pressure was determined using the gold equation of state (EOS): $B_0 = 167.5$ GPa, and $B_0' = 5.79$, whose parameters are obtained with a third-order Birch-Murnaghan equation.[19] The X-ray beam was focused down to 30 × 30 μm^2 using Kickpatrick-Baez mirrors. A pinhole placed before the sample position was used as a clean-up aperture for filtering out the tail of the X-ray beam. The images were collected using a MAR345 image plate located at 350 mm from the sample. The diffraction patterns were integrated as a function of 2θ using FIT2D in order to give conventional, one-dimensional diffraction profiles.[20] The indexing and refinement of the powder diffraction patterns were performed using the Unitcell,[21] POWDERCELL,[22] and GSAS[23,24] program packages.

III. THEORETICAL CALCULATIONS

We have performed *ab initio* total-energy calculations within the density functional theory (DFT)[25] using the plane-wave method and the pseudopotential theory with the Vienna *ab initio* simulation package (VASP).[26] We have used the projector-augmented wave scheme (PAW)[27] implemented in this package to take into account the full nodal character of the all-electron charge density in the core region. Basis set, including plane waves up to an energy cut-off of 520 eV were used in order to achieve highly converged results and accurate description of the electronic properties. The exchange-correlation energy was described with the generalized gradient approximation (GGA) with the PBEsol prescription.[28] A dense special k-points sampling for the Brillouin zone (BZ) integration was performed in order to obtain very well-converged energies and forces. At each selected volume, the structures were fully relaxed to their equilibrium configuration through the calculation of the forces on atoms and the stress tensor. This allows obtaining the relaxed structures at the theoretical pressures defined by the calculated stress. In the relaxed equilibrium configurations, the forces on the atoms are less than 0.006 eV/Å, and deviations of the stress tensor from a diagonal hydrostatic form are less than 1 kbar (0.1 GPa). The application of DFT-based total-energy calculations to the study of semiconductor properties under HP has been reviewed in Ref. 29, showing that the phase stability, electronic, and dynamical properties of compounds under pressure are well described by DFT.

Ab initio calculations allow the study of the mechanical properties of materials. The elastic constants describe the mechanical properties of a material in the region of small deformations, where the stress-strain relations are still linear. The elastic constants can be obtained by computing the macroscopic stress for a small strain with the use of the stress theorem.[30] Alternatively, the macroscopic stress can be also calculated using density functional perturbation theory (DFPT).[31] In the present work, we perform the evaluation of the elastic constants of Tl_2O_3 with the use of the DFT as implemented in the VASP package.[32] The ground state and fully relaxed structures were strained in different directions according to their symmetry.[32] The total-energy variations were evaluated according to a Taylor expansion for the total energy with respect to the applied strain.[33] Due to this fact, it is important to check that the strain used in the calculations guarantees the harmonic behavior. This procedure allows us to obtain the C_{ij} elastic constants in the Voigt notation. The number of independent elastic constants is reduced by crystalline symmetry.[34]

IV. RESULTS AND DISCUSSION

A. X-ray diffraction and structural properties

The crystalline structure of cubic bixbyite-type Tl_2O_3 (see Fig. 1) has two different types of six-fold-coordinated thallium atoms. Thallium located at the 8*b* Wyckoff site has slightly distorted octahedral coordination whilst thallium located at 24*d* Wyckoff site has distorted trigonal prismatic coordination. Finally, oxygen atoms occupy 48*e* Wyckoff sites. From XRD measurements carried out at 1 atm and room temperature outside the DAC, we have made a Rietveld refinement of the lattice parameter and relative

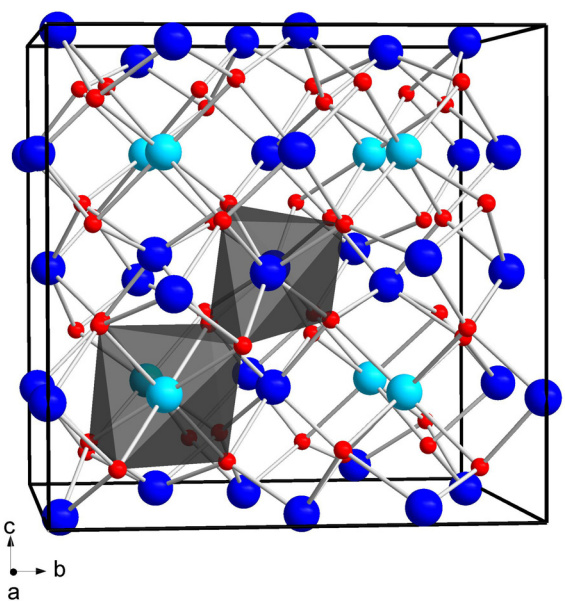

FIG. 1. Schematic representation of the crystalline structure of cubic bixbyite-type Tl_2O_3. The unit-cell and atomic bonds are shown. Oxygen corresponds to small (red) atoms while Tl(1) located at 8*b* and Tl(2) located at 24*d* correspond to light blue and dark blue atoms, respectively.

atomic positions of the bixbyite-type structure. The refinement *R*-values are $R_p = 7.7\%$ and $R_{wp} = 10.2\%$. These results (summarized in Table I) are in quite a good agreement with those of Refs. 2–4, and with our calculations, all of them included in Table I for comparison.

Figure 2 shows ADXRD patterns of Tl_2O_3 up to 37.7 GPa. Diffractograms up to 22 GPa can be indexed with the cubic bixbyite-type Tl_2O_3 structure. The main difference between diffraction patterns up to 22 GPa is the shift of Bragg peaks to higher angles with pressure as the result of a unit-cell volume decrease. A typical peak broadening of XRD peaks[35] is detectable above 11 GPa. In this respect, before continuing the discussion of the results, we would like to comment on possible non-hydrostatic effects in our experiments. We have checked that non-hydrostatic conditions above 11 GPa do not induce a tetragonal or rhombohedral distortion of the cubic structure. As an example, the Rietveld refinement of the powder XRD pattern measured at 18.2 GPa is included in Fig. 2. The refined parameters were: the scale factor, phase fractions, lattice parameters, profile coefficients, *x* fractional atomic coordinate of the Tl(2) atom, the overall displacement factor, and the background. The high quality of the Rietveld refinement shows that Tl_2O_3 remains in the cubic phase at 18.2 GPa; i.e., just before the onset of the amorphization process, as will be explained below. We note that the broadening of XRD peaks above 11 GPa could be due to the loss of quasi-hydrostatic conditions of the pressure-transmitting medium[36–38] or to local distortions caused by the appearance of defects which could be precursors of the pressure-induced amorphization (PIA) that will be commented later on.

From the refinement of the diffraction patterns up to 22 GPa, we obtained the pressure dependence of the Tl_2O_3 lattice parameter. In the Rietveld refinement, the oxygen atomic coordinates were supposed not to vary with pressure due to its small X-ray scattering cross section in comparison to that of thallium atom. Rietveld refinements carried out on HP-ADXRD data for Tl_2O_3 show that the *x* fractional atomic coordinate of the Tl(2) atom up to 22 GPa was similar to that at 1 atm within experimental uncertainty. This result agrees with the weak pressure dependence of this atomic parameter obtained from our theoretical calculations (according to simulations, the *x* fractional atomic coordinate of Tl(2) in Tl_2O_3

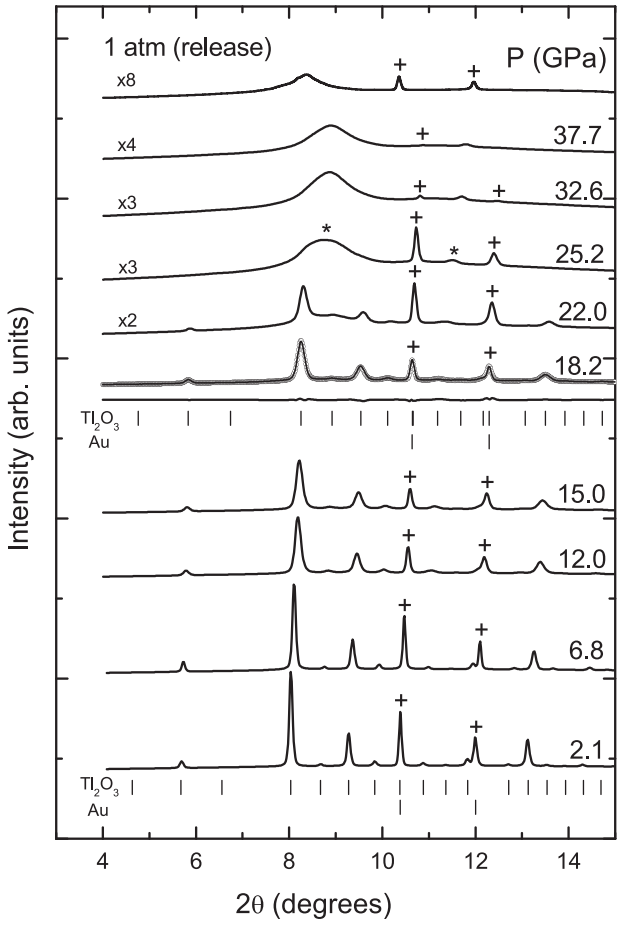

FIG. 2. Room temperature XRD patterns of Tl_2O_3 at selected pressures. The background has not been subtracted. The diffractogram measured at 18.2 GPa is shown as empty circles. The calculated and difference XRD patterns at 18.2 GPa obtained from a Rietveld refinement are plotted with solid lines. The residuals at 18.2 GPa are $R_p = 2.3\%$ and $R_{wp} = 3.0\%$. Bragg reflections from Tl_2O_3 and gold are indicated with vertical ticks at 2.1 and 18.2 GPa. Gold reflections are marked with plus (+) symbols. The XRD pattern at 1 atm after releasing pressure is shown at the top.

TABLE I. Structural parameters of bixbyite-type Tl_2O_3 at 1 atm.

	X-ray diffraction[a]	*Ab initio* PBEsol[b]	Neutron diffraction[c]	X-ray diffraction[d]	Neutron diffraction[e]
a (Å)	10.5390(4)	10.6074	10.543	10.5344(3)	10.5363
Tl(1) site: 8*b*	$x = 0.25$	$x = 0.25$	$x = 0.25$	$x = 0.25$	$x = 0.25$
	$y = 0.25$	$y = 0.25$	$y = 0.25$	$y = 0.25$	$y = 0.25$
	$z = 0.25$	$z = 0.25$	$z = 0.25$	$z = 0.25$	$z = 0.25$
Tl(2) site: 24*d*	$x = 0.969(1)$	$x = 0.9667$	$x = 0.971(4)$	$x = 0.96815(22)$	$x = 0.9657(8)$
	$y = 0$	$y = 0$	$y = 0$	$y = 0$	$y = 0$
	$z = 0.25$	$z = 0.25$	$z = 0.25$	$z = 0.25$	$z = 0.25$
O site: 48*e*	$x = 0.388(5)$	$x = 0.3829$	$x = 0.397(5)$	$x = 0.3824(17)$	$x = 0.3897(10)$
	$y = 0.394(3)$	$y = 0.3885$	$y = 0.377(6)$	$y = 0.3905(15)$	$y = 0.3982(11)$
	$z = 0.148(3)$	$z = 0.1540$	$z = 0.157(5)$	$z = 0.1542(18)$	$z = 0.1431(12)$

[a]Our XRD measurements.
[b]Our calculations.
[c]Reference 2.
[d]Reference 3.
[e]Referernce 4.

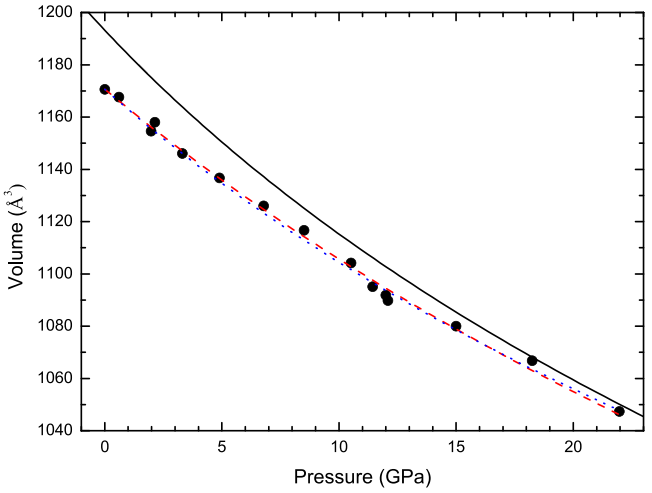

FIG. 3. Evolution of the unit-cell volume with pressure. Symbols refer to experimental data. Error bars are smaller than symbol size. Red dashed line and blue dotted line represent the fit of experimental data with a BM2 and BM3 EOS; respectively. Theoretical results are plotted with solid line.

varies from 0.9667 at 0 GPa to 0.9664 at 22 GPa). The pressure evolution of the unit-cell volume of Tl_2O_3 is plotted in Fig. 3. We have fitted these data with second-order Birch-Murnaghan (BM2) and third-order Birch-Murnaghan (BM3) EOSs.[39] Weights derived from the experimental uncertainties in both pressure and volume were assigned to each data point in both fits. The fits were carried out with the EoSFit software (v.5.2).[40] All the experimental and theoretical values at zero pressure for the volume, V_0, bulk modulus, B_0, and its first-pressure derivative, B_0', are summarized in Table II. Our experimental values are in relatively good agreement with our calculated values. For the case of our experimental data, the obtained value for the weighted chi-squared, χ^2_w, in the BM2 and BM3 EOS fits is 6.2 and 6.7; respectively. We note that, the refinement of the B_0' parameter in the BM3 EOS fit does not improve the fit of the data because the χ^2_w increases to a value of 6.7 and the standard deviation of B_0 increases with respect to that obtained with the BM2 EOS, thus indicating that an expansion of the EOS to third order is not required to fit the data. These results show that the second-order equation of state is an adequate representation of the volume-pressure data of Tl_2O_3. For comparison purposes, the EOS parameters for isostructural In_2O_3 are also included in Table II.[41–43] It can be highlighted

TABLE II. Experimental (Exp.) and theoretical (Th.) EOS parameters for cubic bixbyite-type Tl_2O_3 at zero pressure. Last column indicates the EOS type used (BM2 = Birch-Murnaghan of 2nd order, BM3 = Birch-Murnaghan of 3rd order). Results for isostructural In_2O_3 are included for comparison.

Compound	V_0 (Å^3)	B_0 (GPa)	B_0'	Reference	EOS type
Tl_2O_3 (Exp.)	1170.6(1)	147(13)	5(2)	This work	BM3
Tl_2O_3 (Exp.)	1170.6(1)	156(3)	4 (fixed)	This work	BM2
Tl_2O_3 (Th.)	1193.2(1)	125.0(4)	4.97(4)	This work	BM3
Tl_2O_3 (Th.)	1191.5(5)	134.2(7)	4 (fixed)	This work	BM2
In_2O_3 (Exp.)	1038(2)	194(3)	4.75 (fixed)	41	BM3
In_2O_3 (Exp.)	1035.4(2)	178.9(9)	5.15	42	BM3
In_2O_3 (Exp.)	1028(2)	184(10)	4 (fixed)	43	BM2

that the experimental value for B_0 in Tl_2O_3 ($B_0 = 156(3)$ GPa) is approximately 15% smaller than that obtained for In_2O_3 ($B_0 = 184(10)$ GPa).[43] In this comparison, we considered the EOS parameters obtained with a BM2 EOS with B_0' fixed to 4 because the B_0 and B_0' parameters are strongly correlated.[44] The lower value of B_0 for cubic Tl_2O_3 when compared to that of In_2O_3 is consistent with the decrease of the bulk modulus of bixbyite-type sesquioxides when the ionic radius of the A cation increases in the series A = In, Tl. We note that bixbyite-type sesquioxides like In_2O_3 and Tl_2O_3 are much less compressible than sesquioxides of late group-15 elements in the Periodic Table like cubic α-Sb_2O_3 (S.G.: Fd–$3m$, No. 227, Z = 16)[45] and monoclinic α-Bi_2O_3 (S.G.: $P2_1/c$, No. 14, Z = 4).[46]

Figure 2 shows a drastic decrease of the intensity of the Bragg reflections of cubic Tl_2O_3 between 18.2 and 22 GPa. In addition, at 25.2 GPa, all the sharp crystalline peaks of cubic Tl_2O_3 disappear and two broad peaks appear at 8.75° and 11.53° (noted with asterisk marks). These two peaks remain up to 37.7 GPa, the maximum pressure achieved in our experiment and exhibit a small shift to higher angles between 25.2 and 37.7 GPa. These results can be interpreted as an amorphization of Tl_2O_3 above 22.0 GPa which is already completed at 25.2 GPa and will be discussed in Sec. IV B.

B. Amorphization

It is commonly accepted that PIA in crystalline solids may occur if the crystalline structure becomes mechanical or dynamically unstable at a certain pressure; i.e., if mechanical stability criteria are violated or if the phonon dispersion curves contain imaginary frequencies for phonon modes at a given pressure.[47] PIA due to these instabilities usually occurs when the crystalline solid cannot undergo a phase transition to a HP crystalline phase at a smaller pressure than that of amorphization. The hindrance of the pressure-driven phase transition between two crystalline phases is usually due to the presence of kinetic barriers between the low- and high-pressure structures. This barrier cannot be overcome if the temperature is not high enough and consequently the transition is frustrated at low temperatures. Therefore, it is worth to investigate which could be the frustrated HP phase of Tl_2O_3 and at which pressure the phase transition is predicted to occur.

In order to look for candidates of HP phases of Tl_2O_3, we have performed total-energy calculations for Tl_2O_3 with the structures observed experimentally in In_2O_3 at different pressures and temperatures.[48–52] They include bixbyite-type (Ia–3), corundum-type (S.G.: R–$3c$, No. 167, Z = 6), orthorhombic Rh_2O_3-II-type (S.G.: $Pbcn$, No. 60, Z = 4), and orthorhombic α-Gd_2S_3-type (S.G.: $Pnma$, No. 62, Z = 4) structures. We have also considered in our calculations the orthorhombic Rh_2O_3-III-type structure (S.G. $Pbca$, No. 61, Z = 8), which is a high-temperature and low-pressure form of Rh_2O_3,[53] and two of the structures commonly found in rare-earth sesquioxides (RES) under different pressure and temperature conditions,[54–58] like the monoclinic B-RES (S.G.: $C2/m$, No. 12, Z = 6) and trigonal A-RES (S.G.

P–3*m*1, No. 164, Z = 1) structures. Finally, to complete the study, we have also considered as candidates for HP phases of Tl_2O_3 structures observed in transition-metal sesquioxides at different pressures and temperatures. These structures are the Sb_2S_3-type (S.G.: *Pnma*, No. 62, Z = 4) found in Ti_2O_3,[59,60] the distorted orthorhombic perovskite or $GdFeO_3$-type (S.G.: *Pnma*, No. 62, Z = 4) found in Fe_2O_3 (hematite)[61] and the orthorhombic post-perovskite or $CaIrO_3$-type (S.G.: *Cmcm*, No. 63, Z = 4) found in Mn_2O_3.[62]

The enthalpy difference vs. pressure diagram for the different Tl_2O_3 polymorphs, taking as reference the enthalpy of the bixbyite-type phase, is plotted in Fig. 4. Our calculations predict a phase transition from the bixbyite-type phase (*Ia*–3) to the Rh_2O_3-II-type phase (*Pbcn*) at 5.8 GPa, and from the Rh_2O_3-II-type phase to the α-Gd_2S_3-type phase (*Pnma*) at 24.2 GPa. This sequence of pressure-induced phase transitions for Tl_2O_3 is the same as for In_2O_3.[48,49] The main difference is the phase transition pressures predicted theoretically in both compounds: 5.8 GPa (7–11 GPa) and 24.2 GPa (36–40 GPa) for Tl_2O_3 (In_2O_3).[48,49] The fact that our HP-ADXRD measurements in Tl_2O_3 up to 37.7 GPa do not show evidence of the phase transitions predicted at 5.8 GPa and 24.2 GPa, but an amorphization whose onset is around 22 GPa, suggests that kinetic barriers might be present in the phase transition to the HP phases at room temperature in Tl_2O_3. Note that the phase transition from the bixbyite-type to the Rh_2O_3-II-type structure was observed in In_2O_3 at room temperature above 30 GPa (Ref. 43) and the transition to the α–Gd_2S_3-type structure in In_2O_3 was not observed at room temperature between 1 atm and 51 GPa.[49] In fact, an amorphous halo was observed in In_2O_3 at 51 GPa and room temperature; thus suggesting a PIA in In_2O_3 at room temperature above this pressure. On the other hand, the phase transition in In_2O_3 from the Rh_2O_3-II-type structure to the α–Gd_2S_3-type structure was observed at HP and high temperature.[49] Furthermore, the phase transition pressures in In_2O_3 were observed experimentally close to those theoretically predicted only in HP and high temperature experiments.[48,49] Those works already showed that large kinetic barriers are present in In_2O_3 at room temperature between the bixbyite-type, Rh_2O_3-II-type and α–Gd_2S_3-type structures; therefore, similar barriers are expected to occur for the same structures in Tl_2O_3. In particular, the hypothesis of the kinetic frustration of the pressure-induced phase transition from the bixbyite-type to the Rh_2O_3-II-type structure in Tl_2O_3 will be explored in detail in future simultaneous HP and high temperature experiments on Tl_2O_3, as it was already done for In_2O_3.[48–52] We note that our *ab initio* calculations do not include kinetic energy barriers and therefore the theoretically predicted HP phases for bixbyite-type Tl_2O_3 could be found experimentally in future HP and high temperature experiments where the kinetic energy barriers can be overcome. Finally, we want to stress that Tl_2O_3 remains amorphous after decompression from 37.7 GPa to 1 atm, i.e. PIA in Tl_2O_3 at room temperature is irreversible.

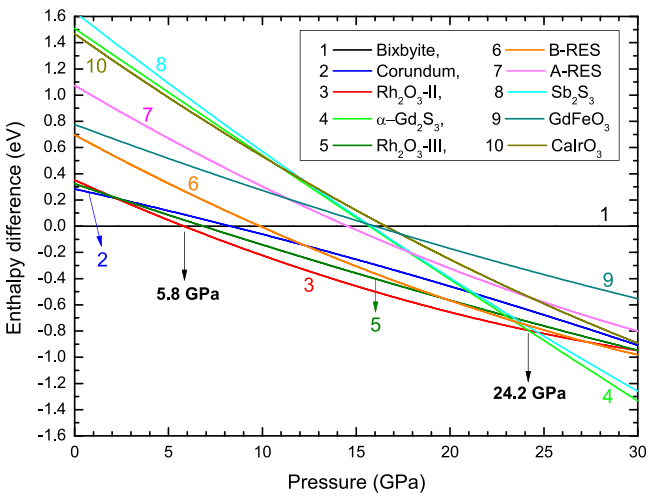

FIG. 4. Theoretical calculation of enthalpy difference vs. pressure for Tl_2O_3 polymorphs. Enthalpy of bixbyite-type phase is taken as the reference. Enthalpy is written per two formula units for all structures for the sake of comparison.

C. Elastic properties

In order to further understand the amorphization process in Tl_2O_3, we have studied the mechanical stability of the cubic bixbyite-type (Ia-3) structure of Tl_2O_3 at HP. This structure belongs to the cubic Laue group CII with point group m-3 which has three independent second order elastic constants: C_{11}, C_{12}, and C_{44}. Table III summarizes the values of the three C_{ij} in Tl_2O_3 at zero pressure as obtained from our *ab initio* calculations. The calculated elastic constants of bixbyite-type In_2O_3 taken from Ref. 63 are also included in Table III for comparison. The values of the three elastic constants of Tl_2O_3 are smaller than those of In_2O_3. This result supports the smaller zero pressure bulk modulus of Tl_2O_3 when compared to that of In_2O_3 as previously commented.

A lattice is mechanically stable at zero pressure only if the Born stability criteria are fulfilled.[64] In the case of cubic systems, these criteria are

$$C_{11} + 2C_{12} > 0, C_{11}–C_{12} > 0, C_{44} > 0. \quad (1)$$

TABLE III. Calculated C_{ij} elastic constants and elastic moduli *B*, *G*, *E* (in GPa) and the Poisson's ratio, ν, for Tl_2O_3 at zero pressure. Elastic moduli and Possion's ratio are given in the Voigt, Reuss and Hill approximations, labeled respectively with subscripts *V*, *R*, and *H*. The *B*/*G* ratio and the Zener anisotropy factor, *A*, are also given. Calculated data at zero pressure taken from Ref. 63 for In_2O_3 are also added for comparison.

	Tl_2O_3[a]	In_2O_3[b]
C_{11}	177.0	234.3
C_{12}	99.2	107.2
C_{44}	32.8	62.7
$B_V = B_R = B_H$	125.1	149.6
G_V, G_R, G_H	35.3, 35.0, 35.1	63.0[c]
E_V, E_R, E_H	96.7, 96.1, 96.4	165.8[c]
ν_V, ν_R, ν_H	0.37, 0.37, 0.37	0.32[c]
$B_V/G_V, B_R/G_R, B_H/G_H$	3.55, 3.57, 3.56	2.37[c]
A	0.84	0.99

[a]Our calculations with GGA-PBEsol prescription.
[b]Calculated with the GGA approximation.
[c]Results calculated in the Hill approximation from reported elastic constants.

In our particular case, all the above criteria are satisfied for bixbyite-type Tl_2O_3 at zero pressure; therefore, cubic Tl_2O_3 is mechanically stable at 1 atm (10^{-4}GPa), as it was expected. When a non-zero uniform stress is applied to the crystal, the above criteria to describe the stability limits of the crystal at finite strain are not adequate and the Born stability criteria must be modified. In this case, the elastic stiffness (or stress-strain) coefficients are defined as

$$B_{ijkl} = C_{ijkl} + 1/2\,[\delta_{ik}\sigma_{jl} + \delta_{jk}\sigma_{il} + \delta_{il}\sigma_{jk} + \delta_{jl}\sigma_{ik} - 2\delta_{kl}\sigma_{ij}], \quad (2)$$

where the C_{ijkl} are the elastic constants evaluated at the current stressed state, σ_{ij} correspond to the external stresses, and δ_{kl} is the Kronecker delta.[65–67] In the special case of hydrostatic pressure applied to a cubic crystal, $\sigma_{11} = \sigma_{22} = \sigma_{33} = -P$, and the elastic stiffness coefficients are: $B_{11} = C_{11} - P$, $B_{12} = C_{12} + P$, and $B_{44} = C_{44} - P$, where P is the hydrostatic pressure. Note that the B_{ij} and C_{ij} coefficients are equal at 0 GPa. When the B_{ij} elastic stiffness coefficients are used, all the relations of the theory of elasticity can be applied including Born's stability conditions which are identical in both loaded and unloaded states.[66–69]

The bulk (B) and shear (G) moduli of cubic Tl_2O_3 can be obtained in the Voigt,[70] Reuss,[71] and Hill[72] approximations, labeled with subscripts V, R, and H, respectively, using the formulae[73]

$$B_V = B_R = \frac{B_{11} + 2B_{12}}{3}, \quad (3)$$

$$B_H = \frac{B_V + B_R}{2}, \quad (4)$$

$$G_V = \frac{B_{11} - B_{12} + 3B_{44}}{5}, \quad (5)$$

$$G_R = \frac{5(B_{11} - B_{12})B_{44}}{4B_{44} + 3(B_{11} - B_{12})}, \quad (6)$$

$$G_H = \frac{G_V + G_R}{2}. \quad (7)$$

In the Voigt (Reuss) approximation, uniform strain (stress) is assumed throughout the polycrystal.[70,71] On the other hand, Hill has shown that the Voigt and Reuss averages are limits and suggested that the actual effective B and G elastic moduli can be approximated by the arithmetic mean of the two bounds.[72] The Young (E) modulus and the Poisson's ratio (ν) are given by[74,75]

$$E_X = \frac{9B_XG_X}{G_X + 3B_X}, \quad (8)$$

$$\nu_X = \frac{1}{2}\left(\frac{3B_X - 2G_X}{3B_X + G_X}\right), \quad (9)$$

where the subscript X refers to the symbols V, R, and H. We summarize in Table III all the values obtained for B, G, E, and ν in bixbyite-type Tl_2O_3 at zero pressure in the Voigt, Reuss, and Hill approximations. Note that our calculated value for the bulk modulus in the Hill approximation ($B_H = 125.1$ GPa) is in very good agreement with the value of $B_0 = 125.0(4)$ GPa obtained from our PBEsol structural calculations via a BM3 EOS fit. This result gives us confidence about the correctness of our elastic constants calculations.

Table III also includes the values of the ratio between the bulk and shear modulus, B/G, and the Zener anisotropy factor, A. The B/G ratio has been proposed by Pugh to predict brittle or ductile behavior of materials.[76] According to the Pugh criterion, a B/G value above 1.75 indicates a tendency for ductility; otherwise, the material behaves in a brittle manner. In our particular case, we found a value of $B/G = 3.56$ in the Hill approximation indicating that the material should be ductile at 1 atm. The Zener anisotropy factor A for our cubic cell is defined as $A = 2B_{44}/(B_{11} - B_{12})$. If A is equal to one, no anisotropy exists. On the other hand, the

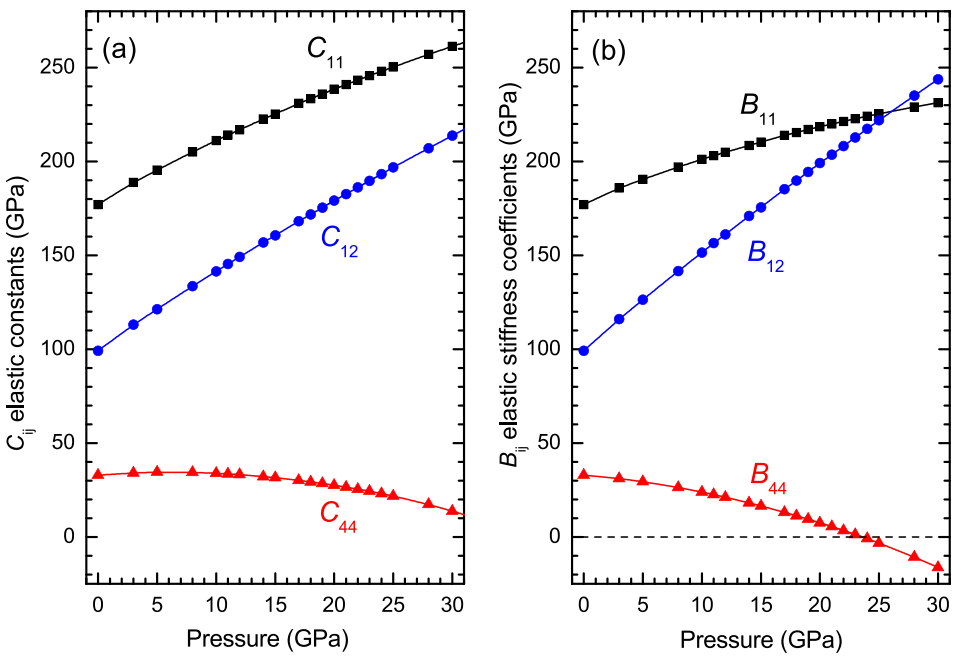

FIG. 5. Pressure dependence of the theoretical (a) C_{ij} elastic constants and (b) B_{ij} elastic stiffness coefficients of bixbyite-type Tl_2O_3. Solid lines connecting the calculated data points are shown as a guide to the eyes.

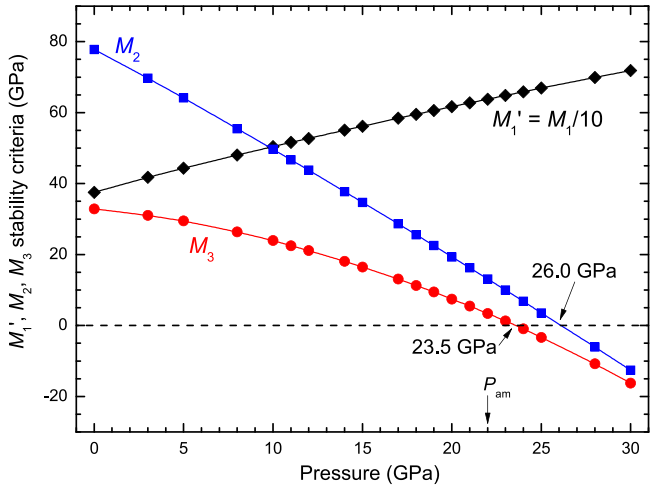

FIG. 6. $M_1' = M_1/10$, M_2, and M_3 stability criteria for bixbyite-type Tl_2O_3 as a function of pressure. The pressure for the onset of the amorphization process, P_{am}, in our experiments is indicated.

more this parameter differs from one, the more elastically anisotropic is the crystalline structure. In cubic Tl_2O_3, the A value (0.84) is slightly different from 1 and evidence a small elastic anisotropy of our cubic cell at 1 atm.

Figures 5(a) and 5(b) show the pressure dependence of the three calculated C_{ij} elastic constants and the three B_{ij} elastic stiffness coefficients of bixbyite-type Tl_2O_3, respectively. It can be seen that B_{11} and B_{12} increase monotonically as pressure increases, while B_{44} decreases monotonically as pressure increases and at 23.5 GPa crosses the 0 GPa horizontal line. This fact is related with the mechanical instability of bixbyite-type Tl_2O_3 and will be discussed in the next paragraphs.

The knowledge of the behavior of the three elastic stiffness coefficients with pressure allows us to study the mechanical stability of bixbyite-type Tl_2O_3 as pressure increases. The new conditions for elastic stability at a given pressure P, known as the generalized stability criteria, are obtained by replacing in Eq. (1) the C_{ij} elastic constants by the B_{ij} elastic stiffness coefficients, and are given by[77]

$$M_1 = B_{11} + 2B_{12} > 0, \tag{10}$$

$$M_2 = B_{11} - B_{12} > 0, \tag{11}$$

$$M_3 = B_{44} > 0, \tag{12}$$

where B_{11}, B_{12}, and B_{14} are the elastic stiffness coefficients at the considered pressure. These generalized stability criteria are plotted in Fig. 6. It is found that Eq. (12), related to a pure shear instability, is violated at 23.5 GPa while Eq. (11), called the Born instability,[77] is violated at 26.0 GPa. Therefore, our theoretical study of the mechanical stability of Tl_2O_3 at HP suggests that the bixbyite-type phase becomes mechanically unstable beyond 23.5 GPa. This pressure is slightly above but very close to the pressure at which the onset of PIA takes place experimentally. Consequently, this result suggests that shear instability could be involved in the PIA process of Tl_2O_3 at room temperature. We want to stress that our calculations are performed for a perfect

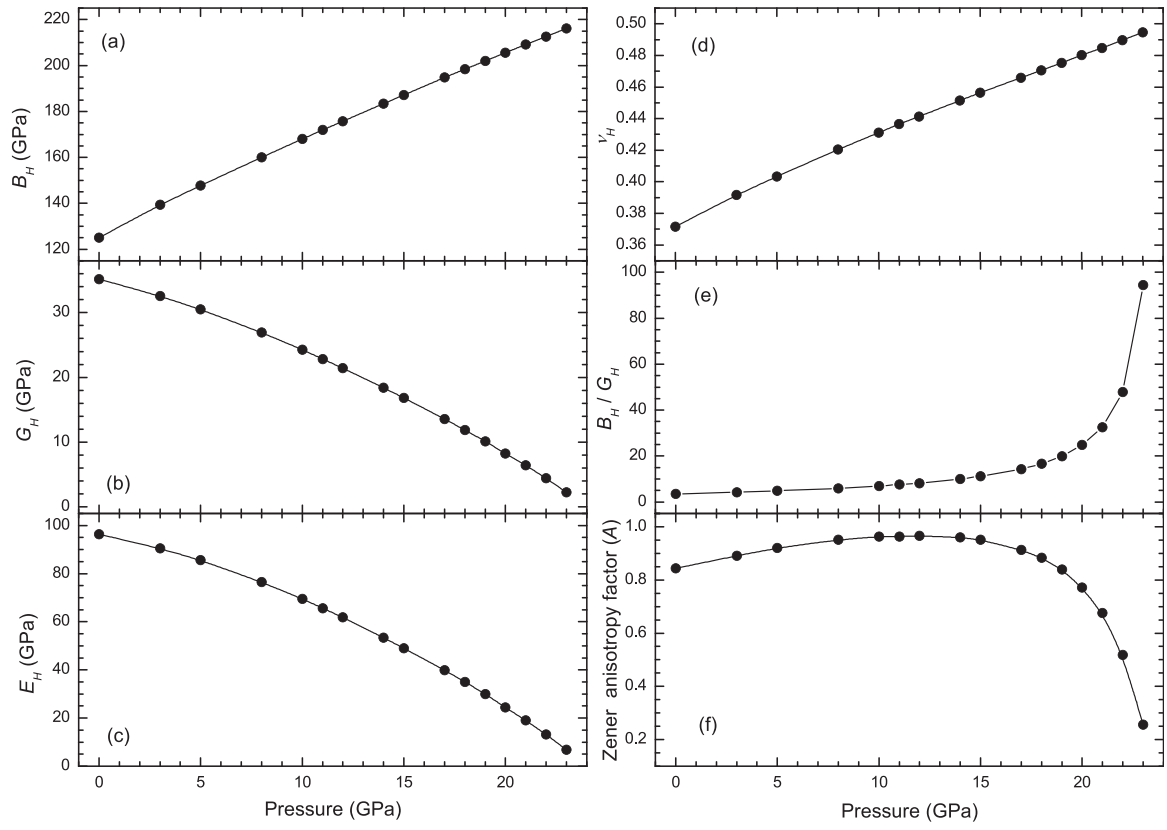

FIG. 7. Pressure dependence of (a) B_H, (b) G_H, (c) E_H, (d) ν_H, (e) B_H/G_H, and (f) A. Solid lines connecting the calculated data points are shown as a guide to the eyes. Results are shown in the Hill approximation.

material, whereas our powder samples are very defective and contain a high concentration of O vacancies that make Tl_2O_3 a degenerate n-type semiconductor. Therefore, we expect that PIA in our sample takes place at a lower pressure than that theoretically predicted since defects are known to induce amorphization and decrease the pressure at which PIA begins in a number of materials.[78,79]

We have also performed the study of the dynamical stability in Tl_2O_3 in order to complement the study of the mechanical stability of Tl_2O_3 and verify that PIA in Tl_2O_3 is caused by the mechanical instability of the cubic phase. To check the dynamical stability of the cubic phase, we have carried out *ab initio* calculations of the phonon dispersion relations in bixbyite-type Tl_2O_3. We have found that the cubic phase is dynamically stable up to 32 GPa and that phonons with imaginary frequencies appear above this pressure. This result thus indicates that bixbyite-type Tl_2O_3 becomes dynamically unstable above 32 GPa.[80] Since this pressure is higher than the pressure at which bixbyite-type Tl_2O_3 becomes mechanically unstable, we conclude that PIA of Tl_2O_3 observed at room temperature at 22 GPa might be caused by the mechanical instability of the cubic lattice at pressures above 22 GPa.

Finally, for completeness we have plotted the pressure dependence of the elastic moduli (B_H, G_H and E_H), ν_H Poisson's ratio, B_H/G_H ratio, and A Zener anisotropy factor in Fig. 7. It is found that B_H increases with pressure and reaches the value of 216.0 GPa at 23 GPa. On the other hand, G_H and E_H decrease with pressure approaching a value of 0 GPa near 23.5 GPa, pressure at which the mechanical instability is predicted to occur. We note that the fact that the shear modulus decreases with pressure is compatible with the fact that the equation that first is violated (Eq. (12)) is the one related with the pure shear instability because of the decreasing of B_{44} with pressure. The Poisson's ratio, ν_H, increases with pressure and reaches a value of 0.49 at 23 GPa. The B_H/G_H ratio increases with pressure, grows exponentially above 19 GPa, and reaches a value of 94.4 at 23 GPa. The increase of the B_H/G_H ratio with pressure indicates that the ductility of Tl_2O_3 is enhanced under compression. In the case of the Zener anisotropy factor, A, it is found that it increases with pressure reaching a maximum value of $A = 0.96$ at about 11 GPa and afterward decreases quickly above 20 GPa indicating a strong increase of the elastic anisotropy above that pressure.

V. CONCLUDING REMARKS

We have studied both experimentally and theoretically the structural properties of Tl_2O_3 under compression at room temperature. The equation of state of Tl_2O_3 has been determined and its bulk modulus has been found to be smaller than that of isostructural In_2O_3. Tl_2O_3 starts to amorphize above 22 GPa and retains the amorphous structure at 1 atm when decreasing pressure from 37.7 GPa. The theoretically predicted transitions to the Rh_2O_3-II-type structure, near 6 GPa, and to the α-Gd_2S_3-type structure, near 24 GPa, are not observed experimentally, probably, due to the kinetic hindrance of the phase transitions at room temperature.

To understand the pressure-induced amorphization process of Tl_2O_3, we have studied theoretically both the mechanical and dynamical stability of the cubic phase at high pressures. In this respect, the mechanical properties of bixbyite-type Tl_2O_3 at high pressures have been commented. Our calculations show that amorphization might be caused by the mechanical instability of the bixbyite-type structure predicted above 23.5 GPa since this phase is dynamically stable up to 32 GPa.

ACKNOWLEDGMENTS

This study was supported by the Spanish government MEC under Grant Nos. MAT2010-21270-C04-01/03/04, MAT2013-46649-C4-1/2/3-P, and CTQ2009-14596-C02-01, by the Comunidad de Madrid and European Social Fund (S2009/PPQ-1551 4161893), by MALTA Consolider Ingenio 2010 project (CSD2007-00045), and by Generalitat Valenciana (GVA-ACOMP-2013-1012 and GVA-ACOMP-2014-243). We acknowledge Diamond Light Source for time on beamline I15 under proposal EE6517 and I15 beamline scientist for technical support. A.M. and P.R.-H. acknowledge computing time provided by Red Española de Supercomputación (RES) and MALTA-Cluster. B.G.-D. and J.A.S. acknowledge financial support through the FPI program and Juan de la Cierva fellowship. J.R.-F. acknowledges the Alexander von Humboldt Foundation for a postdoctoral fellowship.

[1]Kh. N. Karpova, E. A. Kon'kova, E. D. Larkin, and V. F. Savel'ev, Doklady Akad. Nauk. Uzbekistan S.S.R. **2**, 23 (1958).
[2]P. Papamantellos, Z. Kristallogr. **126**, 143 (1968).
[3]H. H. Otto, R. Baltrusch, and H.-J. Brandt, Physica C **215**, 205 (1993).
[4]P. Berastegui, S. Eriksson, S. Hull, F. J. García-García, and J. Eriksen, Solid State Sci. **6**, 433 (2004).
[5]C. T. Prewitt, R. D. Shannon, D. B. Rogers, and A. W. Sleight, Inorg. Chem. **8**, 1985 (1969).
[6]C. R. Patra and A. Gedanken, New J. Chem. **28**, 1060 (2004).
[7]J. A. Switzer, J. Electrochem. Soc. **133**,722 (1986).
[8]R. J. Phillips, M. J. Shane, and J. A. Switzer, J. Mater. Res. **4**, 923 (1989).
[9]R. A. Van Leeuwen, C. J. Hung, D. R. Kammler, and J. A. Switzer, J. Phys. Chem. **99**, 15247 (1995).
[10]R. N. Bhattacharya, "Thallium-oxide superconductors," in *High Temperature Superconductors*, edited by R. N. Bhattacharya and M. Parans Paranthaman (Wiley-VCH, Weinheim, 2010), pp. 129–151.
[11]C. D. Weaver, D. Harden, S. I. Dworetzky, B. Robertson, and R. J. Knox, J. Biomol. Screen **9**, 671 (2004).
[12]H. P. Geserich, Phys. Status Solidi **25**, 741 (1968).
[13]A. Goto, H. Yasuoka, A. Hayashi, and Y. Ueda, J. Phys. Soc. Jpn. **61**, 1178 (1992).
[14]P. A. Glans, T. Learmonth, K. E. Smith *et al.*, Phys. Rev. B **71**, 235109 (2005).
[15]A. B. Kehoe, D. O. Scanlon, and G. W. Watson, Phys. Rev. B **83**, 233202 (2011).
[16]V. N. Shukla and G. P. Wirtz, J. Am. Ceram. Soc. **60**, 253 (1977).
[17]V. N. Shukla and G. P. Wirtz, J. Am. Ceram. Soc. **60**, 259 (1977).
[18]G. P. Wirtz, C. J. Yu, and R. W. Doser, J. Am. Ceram. Soc. **64**, 269 (1981).
[19]M. Yokoo, N. Kawai, K. G. Nakamura, K. I. Kondo, Y. Tange, and T. Tsuchiya, Phys. Rev. B **80**, 104114 (2009).
[20]A. P. Hammersley, S. O. Svensson, M. Hanfland, A. N. Fitch, and D. Häusermann, High Pressure Res. **14**, 235 (1996).
[21]T. J. B. Holland and S. A. T. Redfern, Mineral. Mag. **61**, 65 (1997).
[22]W. Kraus and G. Nolze, J. Appl. Crystallogr. **29**, 301 (1996).
[23]A. C. Larson and R. B. von Dreele, LANL Report No. 86–748, 2004.
[24]B. H. Toby, J. Appl. Cryst. **34**, 210 (2001).
[25]P. Hohenberg and W. Kohn, Phys. Rev. **136**, B864 (1964).

[26]G. Kresse and J. Hafner, Phys. Rev. B **47**, 558 (1993); G. Kresse and J. Hafner, Phys. Rev. B **49**, 14251 (1994); G. Kresse and J. Furthmüller, Comput. Mat. Sci. **6**, 15 (1996); G. Kresse and J. Furthmüller, Phys. Rev. B **54**, 11169 (1996).
[27]P. E. Blöchl, Phys. Rev. B **50**, 17953 (1994); G. Kresse and D. Joubert, Phys. Rev. B **59**, 1758 (1999).
[28]J. P. Perdew, A. Ruzsinszky, G. I. Csonka, O. A. Vydrov, G. E. Scuseria, L. A. Constantin, X. Zhou, and K. Burke, Phys. Rev. Lett. **100**, 136406 (2008).
[29]A. Mujica, A. Rubio, A. Muñoz, and R. J. Needs, Rev. Mod. Phys. **75**, 863 (2003).
[30]N. Chetty, A. Muñoz, and R. M. Martin, Phys. Rev. B **40**, 11934 (1989).
[31]S. Baroni, S. de Gironcoli, A. Dal Corso, and P. Giannozzi, Rev. Mod. Phys. **73**, 515 (2001).
[32]Y. Le Page and P. Saxe, Phys. Rev. B **65**, 104104 (2002).
[33]O. Beckstein, J. E. Klepeis, G. L. W. Hart, and O. Pankratov, Phys. Rev. B **63**, 134112 (2001).
[34]J. F. Nye, *Physical Properties of Crystals. Their Representation by Tensor and Matrices* (Oxford University Press, 1957).
[35]O. Gomis, J. A. Sans, R. Lacomba-Perales, D. Errandonea, Y. Meng, J. C. Chervin, and A. Polian, Phys. Rev. B **86**, 054121 (2012).
[36]D. He and T. S. Duffy, Phys. Rev. B **73**, 134106 (2006).
[37]D. Errandonea, R. Boehler, S. Japel, M. Mezouar, and L. R. Benedetti, Phys. Rev. B **73**, 092106 (2006).
[38]S. Klotz, J. C. Chervin, P. Munsch, and G. Le Marchand, J. Phys. D: Appl. Phys. **42**, 075413 (2009).
[39]F. Birch, J. Geophys. Res. **83**, 1257, doi:10.1029/JB083iB03p01257 (1978).
[40]R. J. Angel, "Equations of state," in *High-temperature and High-Pressure Crystal Chemistry*, MSA Reviews in Mineralogy and Geochemistry, vol. 41, edited by R. M. Hazen and R. T. Downs, (Mineralogical Society of America, 2000), pp. 35–60.
[41]D. Liu, W. W. Lei, B. Zou, S. D. Yu, J. Hao, K. Wang, B. B. Liu, Q. L. Cui, and G. T. Zou, J. Appl. Phys. **104**, 083506 (2008).
[42]J. Qi, J. F. Liu, Y. He, W. Chen, and C. Wang, J. Appl. Phys. **109**, 063520 (2011).
[43]B. García-Domene, J. A. Sans, O. Gomis, F. J. Manjón, H. M. Ortiz, D. Errandonea, D. Santamaría-Pérez, D. Martínez-García, R. Vilaplana, A. L. J. Pereira, A. Morales-García, P. Rodríguez-Hernández, A. Muñoz, C. Popescu, and A. Segura, J. Phys. Chem. C **118**, 20545 (2014).
[44]R. J. Angel, J. L. Mosenfelder, and C. S. J. Shaw, Phys. Earth Planet. Inter. **124**, 71, (2001).
[45]A. L. J. Pereira, L. Gracia, D. Santamaría-Pérez, R. Vilaplana, F. J. Manjón, D. Errandonea, M. Nalin, and A. Beltrán, Phys. Rev. B **85**, 174108 (2012).
[46]A. L. J. Pereria, D. Errandonea, A. Beltrán, L. Gracia, O. Gomis, J. A. Sans, B. García-Domene, A. Miquel-Veyrat, F. J. Manjón, A. Muñoz, and C. Popescu, J. Phys.: Condens. Matter **25**, 475402 (2013).
[47]N. Choudhury and S. L. Chaplot, Phys. Rev. B **73**, 094304 (2006).
[48]H. Yusa, T. Tsuchiya, N. Sata, and Y. Ohishi, Phys. Rev. B **77**, 064107 (2008).
[49]H. Yusa, T. Tsuchiya, J. Tsuchiya, N. Sata, and Y. Ohishi, Phys. Rev. B **78**, 092107 (2008).
[50]A. Gurlo, D. Dzivenko, P. Kroll, and R. Riedel, Phys. Status Solidi (RRL) **2**, 269 (2008).
[51]M. F. Bekheet, M. R. Schwarz, S. Lauterbach, H. J. Kleebe, P. Kroll, A. Stewart, U. Kolb, R. Riedel, and A. Gurlo, High Pressure Res. **33**, 697 (2013).
[52]M. F. Bekheet, M. R. Schwarz, S. Lauterbach, H. J. Kleebe, P. Kroll, R. Riedel, and A. Gurlo, Angew. Chem., Int. Ed. **52**, 6531 (2013).
[53]J. W. M. Biesterbos and J. Hornstra, J. Less-Common Met. **30**, 121 (1973).
[54]L. Wang, Y. Pan, Y. Ding, W. Yang, W. L. Mao, S. V. Sinogeikin, Y. Meng, G. Shen, and H.-K. Mao, Appl. Phys. Lett. **94**, 061921 (2009).
[55]E. Husson, C. Proust, P. Guillet, and J. P. Itié, Mater. Res. Bull. **34**, 2085 (1999).
[56]C. Meyer, J. P. Sanchez, J. Thomasson, and J. P. Itié, Phys. Rev. B **51**, 12187 (1995).
[57]Q. Guo, Y. Zhao, C. Jiang, W. L. Mao, Z. Wang, J. Zhang, and Y. Wang, Inorg. Chem. **46**, 6164 (2007).
[58]Q. Guo, Y. Zhao, C. Jiang, W. L. Mao, and Z. Wang, Solid State Commun. **145**, 250 (2008).
[59]D. Nishio-Hamane, M. Katagiri, K. Niwa, A. Sano-Furukawa, T. Okada, and T. Yagi, High Pressure Res. **29**, 379 (2009).
[60]S. V. Ovsyannikov, X. Wu, V. V. Shchennikov, A. E. Karkin, N. Dubrovinskaia, G. Garbarino, and L. Dubrovinsky, J. Phys.: Condens. Matter **22**, 375402 (2010).
[61]S. Ono, K. Funakoshi, Y. Ohishi, and E. Takahashi, J. Phys.: Condens. Matter **17**, 269 (2005).
[62]J. Santillán, S. H. Shim, G. Shen, and V. B. Prakapenka, Geophys. Res. Lett. **33**, L15307, doi:10.1029/2006GL026423 (2006).
[63]H. Yao, L. Ouyang, and W.-Y. Ching, J. Am. Ceram. Soc. **90**, 3194 (2007).
[64]M. Born, Proc. Cambridge Philos. Soc. **36**, 160 (1940).
[65]D. C. Wallace, "Thermoelastic theory of stressed crystals and higher-order elastic constants," in *Solid State Physics*, edited by F. S. Henry Ehrenreich, D. Turnbull, and F. Seitz (Academic Press, 1970), vol. **25**, pp. 301–404.
[66]J. Wang, S. Yip, S. R. Phillpot, and D. Wolf, Phys. Rev. Lett. **71**, 4182 (1993).
[67]J. Wang, J. Li, S. Yip, S. Phillpot, and D. Wolf, Phys. Rev. B **52**, 12627 (1995).
[68]B. B. Karki, L. Stixrude, and R. M. Wentzcovitch, Rev. Geophys. **39**, 507, doi:10.1029/2000RG000088 (2001).
[69]O. M. Krasil'nikov, M. P. Belov, A. V. Lugovskoy, I. Yu. Mosyagin, and Yu. Kh. Vekilov, Comput. Mater. Sci. **81**, 313 (2014).
[70]W. Voigt, *Lehrbuch der Kristallphysik* (Teubner, Leipzig, 1928).
[71]A. Reuss and Z. Angew, Math. Mech. **9**, 49 (1929).
[72]R. Hill, Proc. Phys. Soc. London, A **65**, 349 (1952).
[73]Z.-J. Wu, E.-J. Zhao, H.-P. Xiang, X.-F. Hao, X.-J. Liu, and J. Meng, Phys. Rev. B **76**, 054115 (2007).
[74]R. Caracas and T. B. Ballaran, Phys. Earth Planet. Inter. **181**, 21 (2010).
[75]Q. J. Liu, Z. T. Liu, and L. P. Feng, Commun. Theor. Phys. **56**, 779 (2011).
[76]S. F. Pugh, Philos. Mag. **45**, 823 (1954).
[77]G. Grimvall, B. Magyari-Köpe, V. Ozoliņš, and K. A. Persson, Rev. Mod. Phys. **84**, 945 (2012).
[78]S. M. Sharma and S. K. Sikka, Prog. Mater. Sci. **40**, 1 (1996).
[79]P. Richet and P. Gillet, Eur. J. Miner. **9**, 907 (1997).
[80]See supplementary material at http://dx.doi.org/10.1063/1.4897241 for *ab initio* phonon dispersion calculations at 0 and 34 GPa.